Size Effect on Mechanical Properties and Mechanical Behavior of Micron-Sized Amorphous Particles

S.O.B Oppong, L. Gyansah and Michael Acquaye

Regional Maritime University, Ghana

DOI: 10.29322/IJSRP.10.09.2020.p105110
http://dx.doi.org/10.29322/IJSRP.10.09.2020.p105110

Abstract- Amorphous micron-sized particles were subjected to a quasi-static compression. A nanoindentation flat punch method has been developed to determine the contact pressure–strain behaviour of single micron-sized amorphous particle. Four groups of particles with same chemical compositions but different diameters were tested. Particle diameters varied from 3.36 µm to 10.05 µm. Three maximum strain levels of 20 %, 30 % and 40 % at constant deformation rate have been applied in the plastic regime. Existing contact mechanics models were discussed and applied to the elastic and plastic regime. The results demonstrate that contact pressure–strain behavior of the amorphous particles in the plastic regime have significant size dependence; the smaller the particle size, the harder the particle behaves. The smaller particles yielded at higher contact pressures. A deflection point that separate elastic regime from plastic regime were observed in the contact pressure-strain curve of the single particle. Cracks in meridian planes exhibit slabbing or axial splitting and seem to be guided around a core structure. A shape pressure drop was observed in the contact pressure-strain behavior of the particle. The elastic range is seen to be much smaller as compared to the plastic range. Stress converges at approximately 4.2 GPa in the plastic-dominant region.

Index Terms- Amorphous particles, size effect, nanoindentation flat tip method, plastic regime

I. Introduction

Significant advancement is achieved in finding and fabricating diversified novel nano materials through the use of nanoindentation. Nanoindentation is currently established tool for investigating the mechanical properties of micro- and nano-scales [1-2]. Recently, micron-sized particles are recently being used in electronic packaging and Anisotropic Conductive Adhesive (ACA) [3-5]. During the indentation process, load–displacement curves are monitored and recorded. Mechanical properties such as hardness, reduced modulus and material stiffness can be computed from the contact area determined by the contact depth using an area function of the indentation tip. However, technical processes such as ceramic processing, powder tableting and fluidization make use of powders of micron-sized particles [6-11]. It has also being found that nanoindentation has profound societal influence on our world economy and socio-economy development in the area of materials and manufacturing, nanoelectronics, medicine and healthcare, energy, biotechnology, information technology, and national security. Recently, there have been other indentation phenomena known as indentation size effect (ISE) [12, 31]. This was revealed more than fifty years ago; however, the mechanisms involved are not fully understood. In indentation size effect theory, hardness measured by nanoindentation for most materials turns to increase with decreasing depth of indentation size within a range typically less than 10 mm. This phenomenon is known as indentation size effect. Particle technology has emerged as one of the research area in the study of mechanical properties, however, the development of it is hindered with great challenges that comprises of development of physical models for engineering systems where particles are in contact [11, 13, 14]. Predictive models are important in designing and modeling of particulate processes for unit operations. The challenge is to prognosticate what mechanical properties such as throughput and energy consumptions can succumb to operational parameters in particulate processes. Such operational parameters have significant effect on the mechanical properties of the particles. There have been some progresses in the determination and purposefulness of particle properties in scientific research. Notwithstanding, probing into mechanical properties of particles such as surface effect, composition, dislocation etc. are still in the neonate stage [12, 15, 16]. Recently, the renowned theory of strain gradient plasticity (SGP) evolved by Nix and Gao [17], surface effect of particles [18], uniform deformed and non-uniform deformed microstructure have received rapid attention. Other functional properties of particles have been modeled using computational fluid dynamics approach and also by means of particle trajectory simulation of particulate systems [14, 15]. Mathematical models that can approximate microsphere in the plastic regime were postulated by Mook et al [14, 19]. Mook et al, approximated the behavior of amorphous particle to that of a barrel shape by a cylinder, an assumptions which works for large deformations [14, 19]. The model considered and accounted for the cylindrical shape and volume conservation which paved way for the contact radius to be computed. This model is popularly known as the Mook model [19]. Another particle technology mathematical model is the Hertzian theory [19, 20-23]. Hertzian theory models high loads and small deformations in the linear elastic regime of isotropic solids. Heinrich Hertz in 1882, successful evolved the first theory of non-adhesive point and line contacts of elastic solids [20-23]. The theory predicts the correlation of engineering equations that mimic particle trajectories and its related mathematical models such as applied load, strain, pressure and contact area and enables the computation of Young's modulus and Poisson's ratio. Hertz assumed a small elliptical contact area between the two solids and approximated

each contact partner by an elastic half-space with a plane surface. The half-space approximation developed by Hertz is habituated to contact mechanics and limited to the application of solutions of elasticity theory. Nonetheless, the model of Oliver and Pharr was developed for the application in traditional nanoindentation experiments and did not considered any significant effects generated by the particle shape and its finite volume [24, 25]. However, there were limitations to O1iver and Pharr model. These limitations were curtailed by the introduction of the Johnson's model [1, 19, 26, 30]. Johnson model accustomed Hertzian theory to anatomize the unloading process to limit complications that may appear at large deformations due to interference of the contact stress fields. Other models such as Abbott and Firestone model [19, 27], Etsion model [19, 28] and Li model [19, 29], offer similar solutions to the limitations of the Oliver and Pharr model. In those models, it was assumed that fully plastically deformed microsphere loaded with a maximum force, will recover elastically when unloaded and the particle will increase effective radius of curvature due to plastic deformation. Their solution is universal for nanoindentation process comprising of the loading and unloading processes. In the last decades, size effect of mechanical properties of PS-DVB micron-sized polymer particles in the elastic regime has been studied by He et al [32].1n this paper, we focus on size effect in the plastic regime on mechanical properties and mechanical behavior of amorphous particles. Amorphous particles are taking trend now in particle technology. According to Paul J etal [7], the mechanical properties of a single particle have significant structure-property correlations. Crack propagation happened when particles were subjected to significant increase in load without particles separating into pieces [7]. Paul J et al found out that crack propagation through the particle is strongly size dependent. However, despite the aforemensioned applications of particle technology, mechanical properties and mechanical behavior of a spherical micron-sized particle are mostly unknown. Unlike other bulk materials, where stress-strain behavior are mostly known, particle dynamics and it associated stress-strain behaviors are unknown. It is therefore pertinent to study structure-property correlations of individual particles and model the behavior of such particles. In this paper, nanoindenter machine was used to probe the mechanical properties of the single particle at different particle sizes. We employed the Hertz and Mook models [13, 14, 21] to study the size effect and mechanical behavior of the particles. The procedure to characterize the mechanical particle properties consist of localizing the position of individual particles and the application of micron or nano-forces to cause deformation to the particles [33-37]. The objective of this paper is to study size effect plastic regime on mechanical properties and mechanical behavior of micron-sized amorphous particles. Amorphous micron-sized particles on a silica substrate were subjected to a quasi-static compression. A nanoindentation flat punch method have been developed to determine the contact pressure–strain behaviors of single micron-sized amorphous particle. Four groups of particles with same chemical compositions but different diameters were subjected to micro-compression. Particle diameters varied from 3.36 µm to 10.05 µm. Three maximum strain levels of 20 %, 30 % and 40 % at constant deformation rate have been applied in the plastic regime at a quasi-static strain rate of 0.025 and 0.05/s mainly to observe the size effect. Existing contact mechanics models were discussed and applied to the elastic and plastic regime.

II. Experimental Setup

1.1.1. Sample Preparation and Methods Used

The Amorphous micron-sized particles used for the experiment were obtained from Xiamen University and were used as received. Energy dispersive spectroscopy (EDS) was conducted to ascertain the chemical elements of the particles (Fig.1.). Table 1 shows the chemical elements of the particle. The Amorphous particles consist of Iron as major element and Silicon, Cobalt, Copper and Niobium as minor chemical elements.

A 12 mm x 12 mm x 0.5 mm Silicon substrate were cleaned in Ethanol and Acetone using high frequency ultrasonic vibration. A 2 mg of micron-sized particles were measured using weight balance machine and dispersed in an Ethanol for 10 minutes. At exactly 10 minutes, drops of the solution containing the particles were dispersed on a 12 mm x 12 mm x 0.5 mm Silica substrate and the diluted dispersions were exposed to ultrasonic vibration to reallocate the positions of the particle array. The Silicon substrates are positioned in a clean environment for thirty minutes for amble drying of the particle in respect to the removal of the remaining Ethanol left in the particles before scanning electron microscopy (SEM) observation. The particles were sputter-coated to initiate conductivity prior to SEM analysis. The SEM micrographs of the smallest and larger particles are illustrated in Fig.2a. Several particles were polished using P5000 abrasive paper and the internal morphologies of particles were observed with SEM and electronic microscope before mechanical testing (Fig.2b, c and d). The observed polished microspheres (Fig.2b) in epoxy no evidence of core-shell feature, no hollow feature, indicating that the particle is not a balloon and no internal cracks (Fig.2c and d) were observed within the particles. Four groups of particles with identical chemical compositions but different diameters have been tested. The diameters of the Amorphous particles varied from 3.36 µm to 10.05 µm. The particles with aspect ratio *(i.e.* Sphericity*)* and *C.V.s (i.e.* coefficient of variance*)* of the size distributions were measured to be one and zero respectively. 4.37 µm particles were also cleaned with Ethanol and subjected to microcompression to observe the mechanical behavior. Differential Scanning Calorimetry **(**DSC**)** tests were performed on the particle. For DSC experiment (Fig.3.), Aluminum pan of melting temperature (T_m) of 660 ˚C were selected as a reference material. A constant cooling and heat rate of 20 K/min were used for the DSC experiment. The room temperature was 22.49˚C. DSC-2000 Machine was used for the experiment. It has a temperature limit of 750˚C. DSC test shows the particle is Amorphous.

Table 1. Major and Minor Elements of the Tested Particles

Chemical Elements	Composition (wt %)

Si	6.40
Fe	70.31
Co	10.72
Cu	14.83
Nb	1.39
Total	100 %

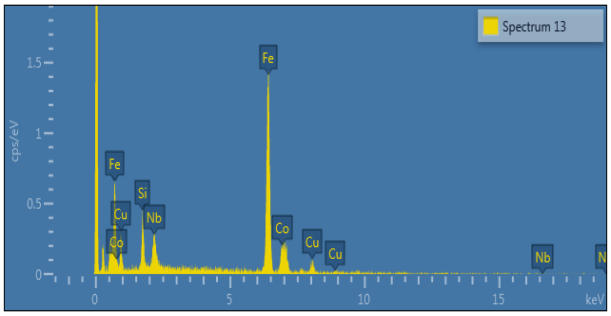

Fig. 1. EDS image of the particle after polishing as a confirmation of the Chemical Elements in Table 1

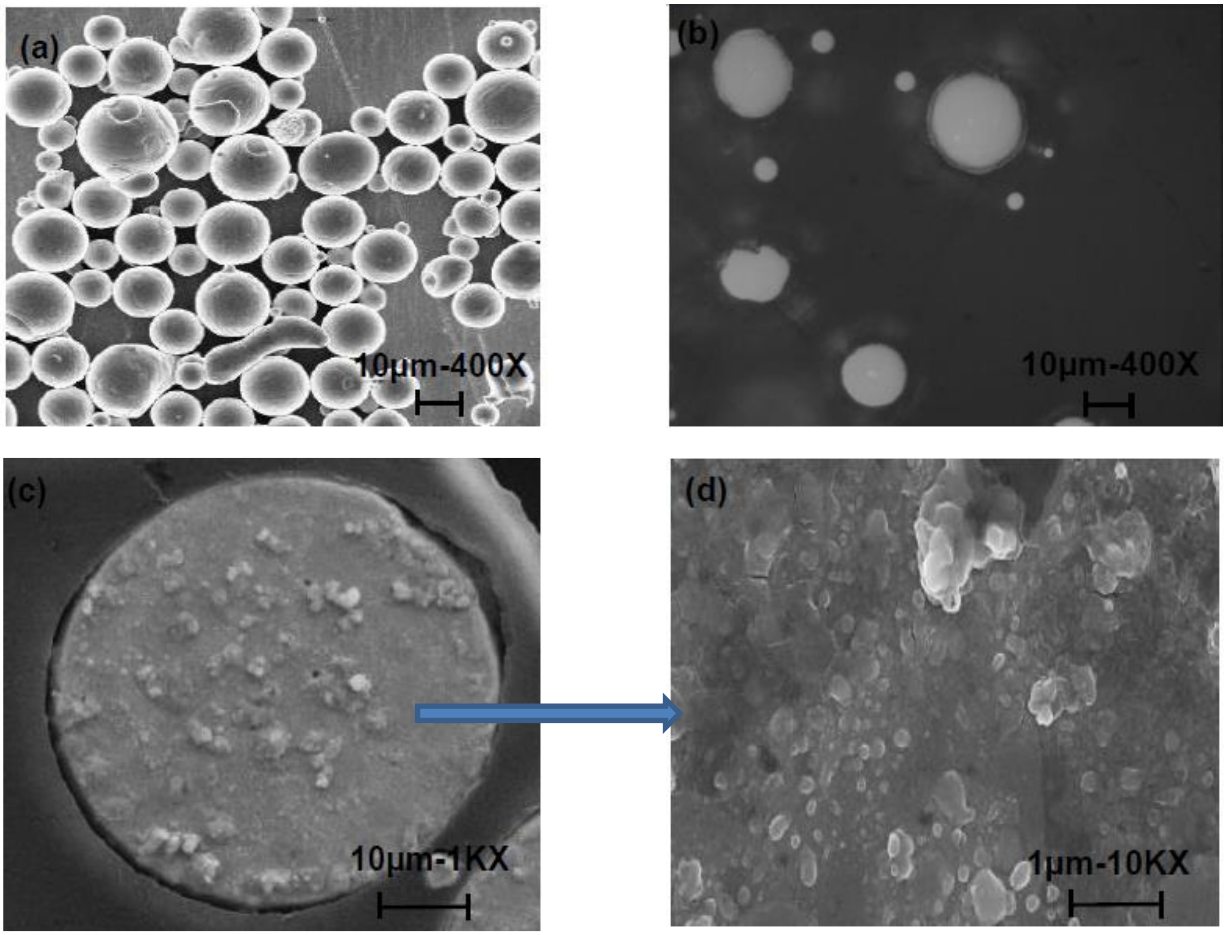

Fig. 2. (a) SEM Micrographs of the smallest particles, broken particles and largest particles (b) Polished microspheres in epoxy no evidence of core-shell feature (c) Polished microsphere shows no hollow feature, indicating that the particle is not a balloon. (d) No internal cracks were observed within the particles.

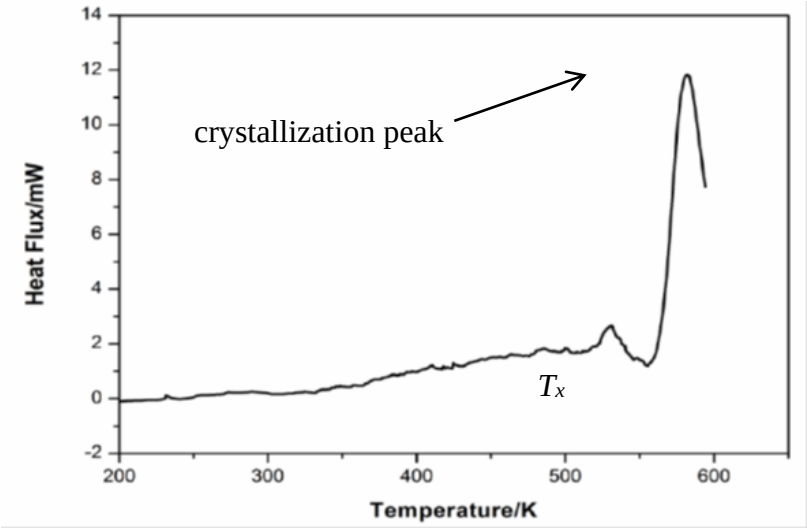

Fig. 3. Shows the DSC Curve for 21mg particles. The crystallization temperature T_x is also characterized by crystallization peak. T_x was measured to be 562.17 ˚C. Crystallization temperature and the crystallization peak are characteristics of amorphous material. This confirms that the particle is Amorphous. The particle did not show any meaningful glass transition.

The microcompression tests are performed using an Agilent Nano Indenter G200 (Agilent Technologies, Inc. 2013, USA). Agilent Nano Indenter G200 is user-friendly instrument for nanoscale mechanical testing. It has the depth-control mode and strain-control mode features. For this experiment, the depth-control mode was utilized. The depth-control mode is controlled by the indentation depth. The depth-control mode has a maximum indentation depth of 2 µm and a maximum load capacity of 500 mN. It has displacement and load resolution of 0.01nm and 50 nN respectively. A flat tip diamond indenter of size 50 µm was used for the experiment. To achieve unparalleled dynamic range in force and displacement, the indenter planarity has to be calibrated. This is achieved by indenting severally into a polished aluminum surface. For experimental certainty, a clean 50 µm impression on the surface of the aluminum is a threshold for planarity acceptability. Once planarity of the indenter tip is achieved, the flat tip indenter is cleaned from dust for mechanical testing to begin. The optical and it position is also calibrated by observation of its resolution on the indent surface of the aluminum. Using the optical microscope, an appropriate distance greater than 50 µm between two particles is observed and a single particle is located for the commencement of the mechanical microcompression test. A schematic diagram (Fig.4.) shows a model of a rigid flat punch in contact with a single amorphous particle. Schematic Plots (Fig.5.) of the particle behavior at different stages which describe the Hertzian and Mook model. The Mook model [14, 19] was used to analyze the contact pressure-strain curves since it is valid in the plastic regime where strain (Ɛ>0.1).

All microcompression tests were performed at room temperature (24 ˚C). The displacement controlled mode which operates the indentation depth versus time is selected in order to control the nominal strain rate for each group of particles. Strain rates were 0.05/s and 0.025/s at speed of 10 nm/s, peak hold is 2s for creep, loading and unloading time is 3 minutes, 20 seconds. Total indentation depth is 2000 nm for all selected particles.

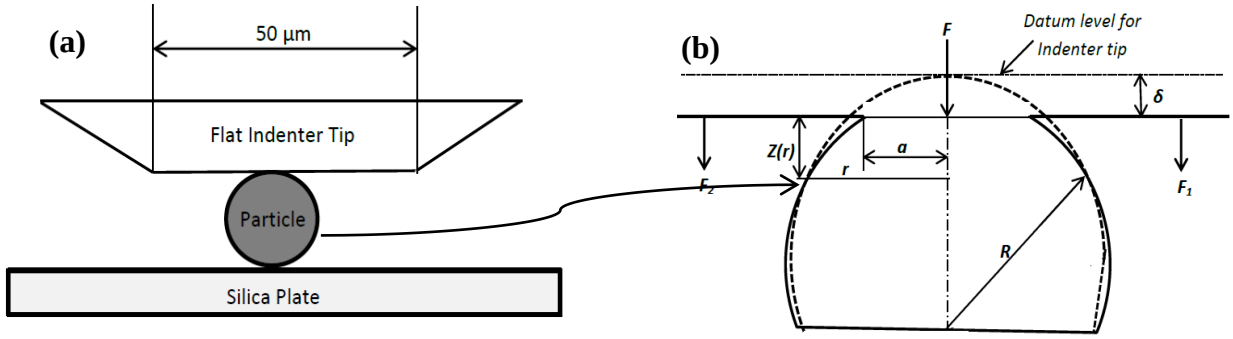

Fig. 4 (a) Model of Flat Punch Test and (b) Enlarged Model Description of Particle

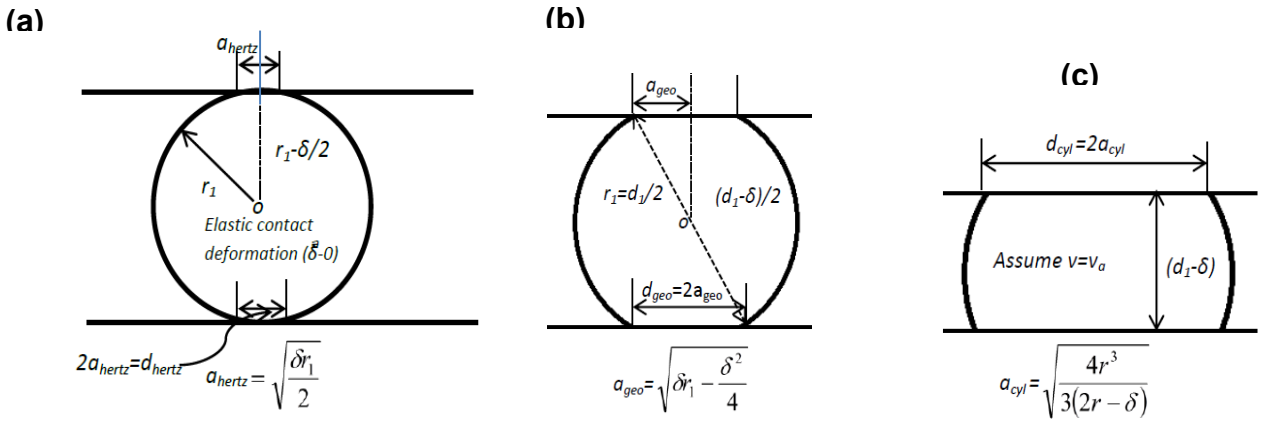

Fig. 5. Schematic Plot of the particle behavior at different stages (a) Hertzian model is valid in elastic regime where strain (Ɛ<=0.1) only, (b) and (c) Mook model valid in the plastic regime where strain (Ɛ>0.1).Where the particle turns to be more barreled shaped. Indication of ductile failure in particle deformation.

After compression of individual particles, two deformation levels 30 % and 40 % were applied in the plastic regimes which correspond to strain rates of 0.025/s and 0.05/s with reference to particle diameter. For mechanical behavior of 4.37 µm, a quasi-static strain rate of 0.05/s was used. Hundreds of particles have been compressed to ascertain the accuracy of the results. All particles were compressed to indentation depth of 2000 nm.

III. Results and Discussion

Force–displacement curves are obtained for all selected amorphous particles at two quasi-static strain levels of 0.025/s and 0.05/s at same indentation depth of 2000 nm respectively as shown in Fig.6 (a) and (b). In Fig. 6 (a), the particles were compressed to a maximum indentation depth of 2000 nm and the experiments were repeated severally to ascertain it accuracy. In Fig. 6 (b), the particles were also subjected to a maximum indentation depth of 2000 nm and the tests were repeated periodically for experimental certainty. It could be seen that the force-displacement behaviors of Fig.6 (a) and (b) for all four different sizes of particles are quite similar, repeatable and consistent. As compared to typical bulk amorphous materials, disparities in microstructure, anisotropy and molecular weight can caused significant variations in mechanical properties [38-40]. Hence, the coherent force–displacement curves substantiated by individual particle at the same indentation depths denote a very homogeneous material including size distribution, microstructure, composition and molecular weight. In addition, it denotes confidence to the experimental certainty and precision. During the microcompression, the volume and poisson's ratio of the amorphous particles may change incessantly with the strain because of the spherical geometry. Therefore, the Mook model [14, 19] which satisfies microspheres in both the elastic and plastic regime was employed to model the behavior of the amorphous particles. To compare the mechanical properties of particles with different sizes, the geometric Mook model equation (Fig.5b) that models contact pressure–strain behaviors of amorphous microspheres have been used. The Mook model is applicable to amorphous particles compressed at strain greater than 10 %. The model is shown in equation (1) and (2).

$$P_C = \frac{P}{\pi a_{geo}^{\ 2}}, \text{where } a_{geo} = \sqrt{\delta r_1 - \frac{\delta^2}{4}} \quad (1)$$

$$\varepsilon_p = \frac{2\delta}{D} = \frac{\delta}{R} \quad (2)$$

Where P_c *is* the contact pressure, ε_p is the nominal compressive strain, *P* is the contact load, *D* is particle diameter, *R* is the initial particle radius, and δ is the half deformation of the spherical amorphous particle (Fig.4 (b)). Fig.7. (a) and (b) shows deflection points that were observed for onset of plasticity/yielding. These points are indicated as *A, B, C* and *D* for 3.36 µm, 4.39 µm, 7.19 µm and 10.05 µm for 0.025/s and 0.05/s. Deflection points were taken as onset of plasticity, so that size effect is studied after the deflection points. The deflection points separate elastic-plastic regime from the plastic regime for each particle size. The contact pressure–strain curves of the four groups of particles at two strain rates are displayed in Fig. 8 (a) and (b), respectively. The unloading part which is purely elastic in nanoindentation experiments has been omitted in the contact pressure-strain behaviors Fig. 8 (a) and (b). From the contact mechanics studies, contact pressure-strain behaviors are one of the constitutive mechanical properties of materials. For particles with different sizes but same chemical compositions, same indentation depth and same strain rate, all the contact-pressure–strain curves should collapse into one phase. Fig. 8 (a) and (b) clearly shows that the smaller particles yielded at higher contact pressures than bigger particles. Contact pressure-strain behaviors of particles at 20 %, 30 % and 40 % in the plastic regime are strongly size-dependent, the smaller the particle size, the harder the particle behaves. The smallest particle is the hardest because it is

characterized by higher contact pressure, while the biggest particle is the softest. As particle size increases, the size dependence in the plastic regime of contact pressure–strain behavior diminishes gradually.

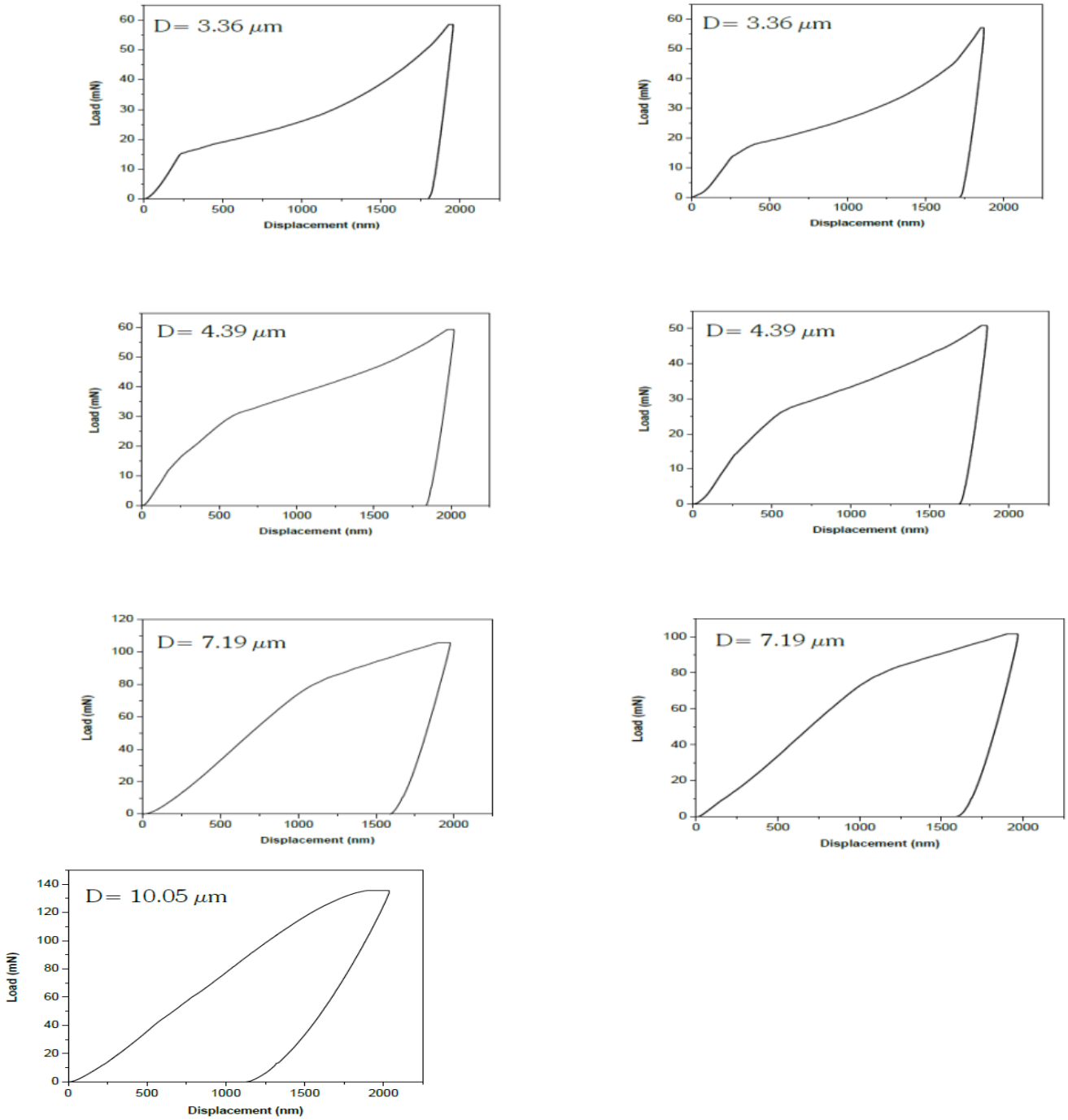

Fig. 6. Force-displacement curves of four different sizes of particles (a) With strain rate 0.05/s at 2 μm indentation depth (b) With strain rate 0.025/s at 2 μm indentation depth.

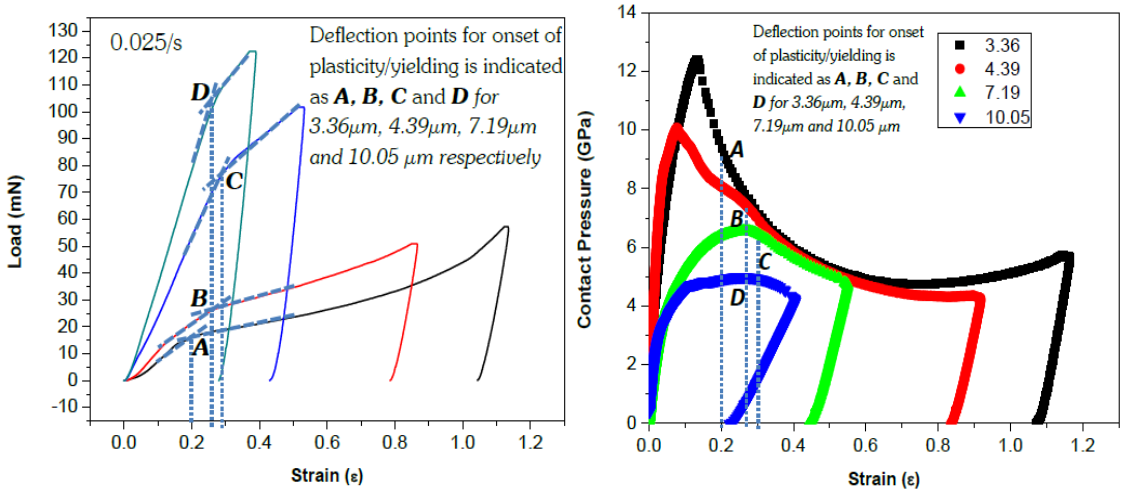

Fig. 7. (a) and (b) Deflection points for onset of plasticity/yielding is indicated as A, B, C and D for 3.36μm, 4.39μm, 7.19μm and 10.05 μm for 0.025/s and 0.05/s. Deflection points were taken as onset of plasticity, so that size effect is studied after the deflection points. The deflection points separate elastic-plastic regime from the plastic regime for each particle size.

Fig.9. Contact pressure-strain curves (a) at 30 % deformation with strain 0.05/s strain rate (b) at 40 % deformation with strain rate 0.025/s. For particles with different sizes but same chemistry and the same strain rate, at 30 % and 40 % deformation in the plastic regime, all the stress-strain curves should collapse into one phase. But Fig.9 (a) and (b), clearly show that the contact pressure-strain behaviors of particles are strongly size-dependent, the smallest particle is the hardest while the biggest particle is the softest. With the increase of particle size, the size dependence of contact pressure-strain behavior diminishes gradually. Fig.9 (a) and (b) indicates that smaller particles size shows higher contact pressure than bigger particles. From Fig.10., particle size dependence of the normalized contact pressure with strain rate 0.025/s and 0.05/s respectively at deformation level 20 %, the contact pressure of all the four groups of particles at 20 % deformation level in the plastic regime is normalized by the corresponding value of the smallest particle. Particles display distinct size effect at both strain rates. The contact pressure of the biggest particle is about 50 % lower than that of the smallest particle at a strain rate of 0.025/s. As the strain rate increases to 0.05/s, the size effect becomes even more pronounced in the plastic regime. The size effect seems to have different trends depending on the strain rate. With the smaller strain rate, the size effect is most evident for the three smaller particle sizes, whereas for the larger strain rate the size effect is more evenly distributed.

There are dissimilarities in the compression modes of failure in amorphous particles compared to their bulk counterpart due to the absence of dislocations [41]. There are three types of compression modes of failure in amorphous particles [1, 2]: Slabbing or axial splitting, crazing or shear banding and microcracking [34, 42, 43]. Slabbing or axial splitting occurs in the absence of confining pressure, where the cracks seems to be initiated parallel to the applied compressive stress. At moderate confining pressure, cracks nucleate within the material to form a "shear zone" [42, 43]. For crazing, a displacement develops tangentially to the surface of displacement. At high confining pressures, distributed microcracking is in evidence. For microcracking, failure occurs as a series of multiple shear fractures distributed throughout the sample volume with no specific crack orientation [1, 2]. The material is said to be "ductile" due to the similarity of shape of the uniaxial stress-strain curve with that obtained on tests with ductile materials. In ductile fracture, extensive plastic deformation takes place before fracture [42]. Ductile behaviors exhibit a deflection point followed by strain softening, usually associated with crazing or shears banding which leads to ductile fracture. It is also delineated by a sharp pressure drop or a plateau in the contact pressure–strain curve [Fig.13]. In brittle fracture, no apparent plastic deformation takes place before fracture [1, 2]. Brittle fracture is depicted by invisible yield point and follows Hooke's law specifically at low strain level. In microcompression tests, compressive failure of amorphous particles is characterized by "barreling" and failure is due to yielding, which can be characterized by the compressive yield strength of the material [Fig.11] and [Fig.12]. Generally, the compressive yield strength for amorphous particles does not change significantly with varying loading mechanisms and can be regarded as a material property.

In [Fig.11.], a 4.37 μm amorphous particles were microcompressed to a maximum strain of 0.96, after microcompression, microspheres show cracks in meridian planes. Cracks in meridian planes were slabbing or axial splitting and seem to be guided around a core structure that is attributed to the synthesis process. The crack features were indicated by *D*, *E*, *F*, *G*, *H*, and *I* [Fig.11]. The particle turns to be more barreled-shaped, which is an indication of ductile failure in particle deformation. Investigation on the compressed load-depth curve [Fig.12], we observed a deflection point which separate elastic-plastic regime from the plastic regime. Three stages in the mechanical behavior of particle were seen [Fig.12]. Stage (1) on the load-strain curve [Fig.12] shows nose effect of the indenter tip. Due to the geometry of the indenter tip, method of attachment, and boundaries of each contacting bodies, nose effect in microcompression of particles are bound to occur [2]. Although, the contacting bodies (i.e the particle and indenter tip) are in frictionless contact, nose effect is just the starting point of the microcompression test. It may cause uncertainties in nanoindentation experiments. However, it could

be seen in [Fig.12.] that the nanoindentation test started exactly at origin, which is indicates nose effect is minimized in this experiment. That is, only a non-uniform pressure is transmitted between the indenter tip and the particle at that stage [1, 2]. Stage (2) is elastic-plastic deformation stage [Fig.12]. At that stage, the behavior of the particle is non-linear [Fig.14]. A deflection point was observed that separate the elastic-plastic from the plastic region. The elastic-plastic stage happens within a strain limit of 0 to 0.27 [Fig.12]. At that stage, a non-uniform pressure distribution exist which might have caused initiation of crack [1, 2]. Stage (3) is dominantly plastic deformation stage. This plastic regime occurs after the deflection point. As indicated in the contact pressure-strain curve [Fig.12] and [Fig.13], as compressed depth increases the elastic-plastic regime is seen to be much smaller as compared to the plastic regime. The elastic-plastic deformed zone (2) decreases with increasing strain and become much smaller than the zone with plastic deformation. The mean contact pressure decreases at this stage [2]. In a plastic dorminant regime, a uniform pressure distribution exists [1, 2]. Stress converges at approximately 4.2 GPa in the plastic-dominant region [Fig.13]. The early stages of (2) shows a sharp pressure drop with no evidence of pop-in event within a strain limit of 0.1 and 0.2 which lies in the Hertzian first pop-in regime [21, 22]. Pop-in events in bulk amorphous materials are an indication the material is yielding [7, 34], however, the fact that the amorphous particle did not experience pop-in events does not mean the material is not plastically deformed. Due to the material composition and dislocation free in some amorphous particles, pop-in event may not happen. The particle completely fractured at a strain of 0.91 [Fig.13] and [Fig.11 (c)] starting from a peak stress of 10 GPa. The final mean contact diameter of the fractured particle was measured to be 2.8 µm using SEM [Fig.14].It was substituted into the geometric Mook model to generate the behavior of the particle. The true behavior of the particle measured in SEM was then compared to the cylindrical Mook model and Hertz model. It could be seen that the contact diameter measured in SEM shows almost the same behaviour as compared to the Mook model and Hertz model [Fig.14]. The graph of cylindrical Mook model d_{cyl} [Fig.14], which indicates that the particle is in the plastic dominant regime, the graph was observed to be linear in both stages (2) and (3) within strain limits of 0 to 0.27 and 0.27 to 0.96 respectively. An indication that means that uniform pressure distribution exists and the particle is deforming plastically. However, no shear bands were observed during deformation. At that point, the particle assumes a barrel shape [Fig.11. (C)]. The graph of geometric Mook model d_{geo} [Fig.14], which is a model that is used to predict the behaviour of a particle in elastic-plastic and plastic regime, shows that at elastic-plastic deformation stage (2), the contact diameter of the particle increased with increase in strain delineated by non-linear behavior. However, stage (3) shows a linear behavior that means the particle is plastically deformed. The graph of the Hertz model d_{hertz} [Fig.14], which is a model that is used to predict the behavior of a particle in elastic-plastic regime only, it was obvious in stage (2) that the behaviour of the particle is non-linear within strain limits of 0 to 0.27. That confirms that the particle is still in the elastic regime and therefore a non-uniform pressure distribution dominate in that region. However, d_m, contact diameter measured in SEM, [Fig.14], reveals that in the plastic domain region (3), the contact diameter of the particle changes almost linearly with the strain (this is where the particle takes the barrel shape). It is a plastically dominant regime where compressive stresses converged at 4.2 GPa. At that point, plasticity would have remained constant at 4.2 GPa and free volume annihilation might have occurred. In stage (2) [Fig.14], a polynomial (non-linear) behavior was observed whilst stage (3) depict that of a linear behavior. However, the Mook model did not fit exactly with the contact diameter measured in SEM. The reason may be experimental uncertainties. The true behavior of the particle is made up of non-linear in the elastic-plastic regime characterized by linear behavior in the plastically dominant region [Fig.14].

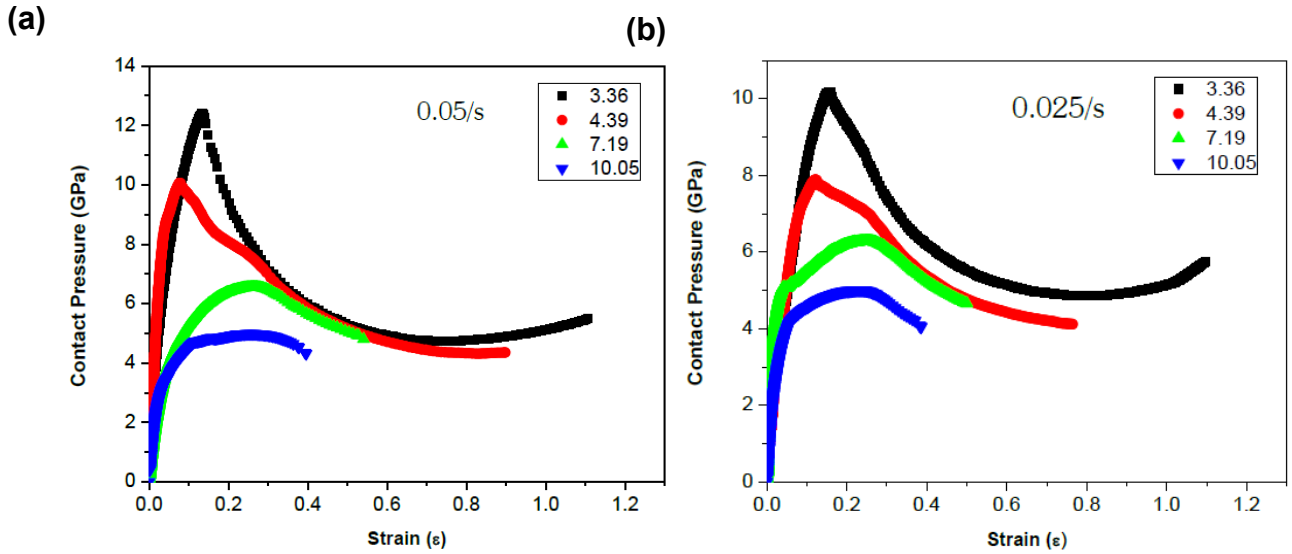

Fig. 8. Contact pressure-strain behaviors of particles exhibiting size-dependent at (a) 0.05/s and (b) 0.025/s respectively.

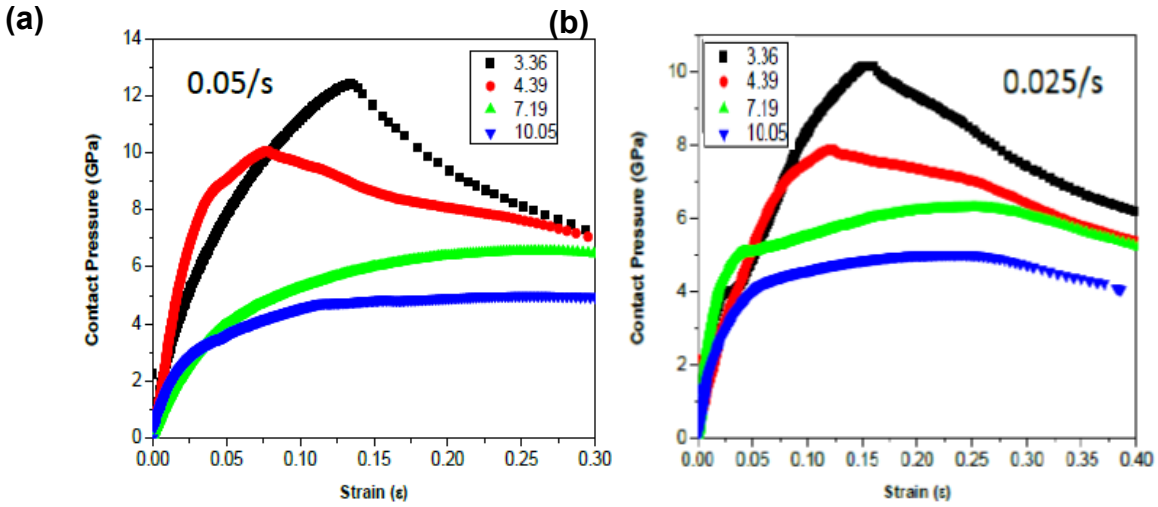

Fig.9.Contact pressure-strain curves (a) at 30 % deformation with strain 0.05/s strain rate (b) at 40 % deformation with strain rate 0.025/s. Both graphs show size effect in the plastic regime.

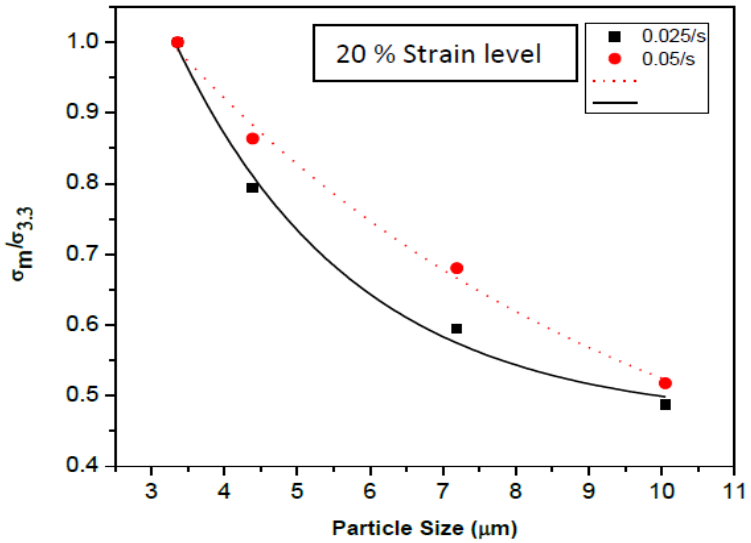

Fig. 10. Particle size dependence of the normalized contact pressure with strain rate 0.025/s and 0.05/s at deformation level 20 %.

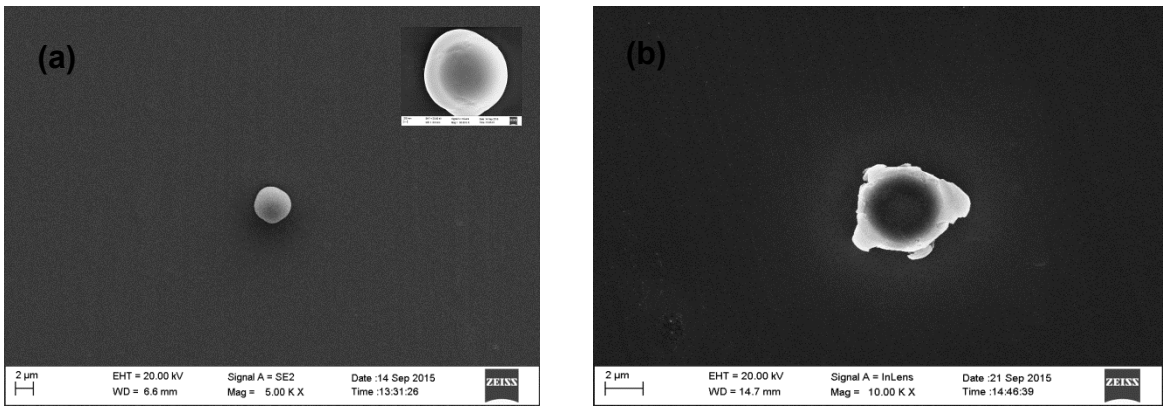

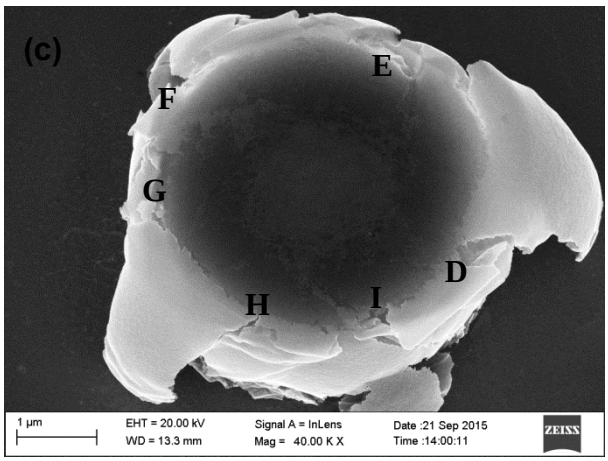

Fig. 11. (a) Particle before test (b) and (c) The particle were loaded to a maximum strain of 0.96, after compression, microsphere barreled and show cracks in meridian planes as indicated by *D*, *E*, *F*, *G*, *H* and *I*.

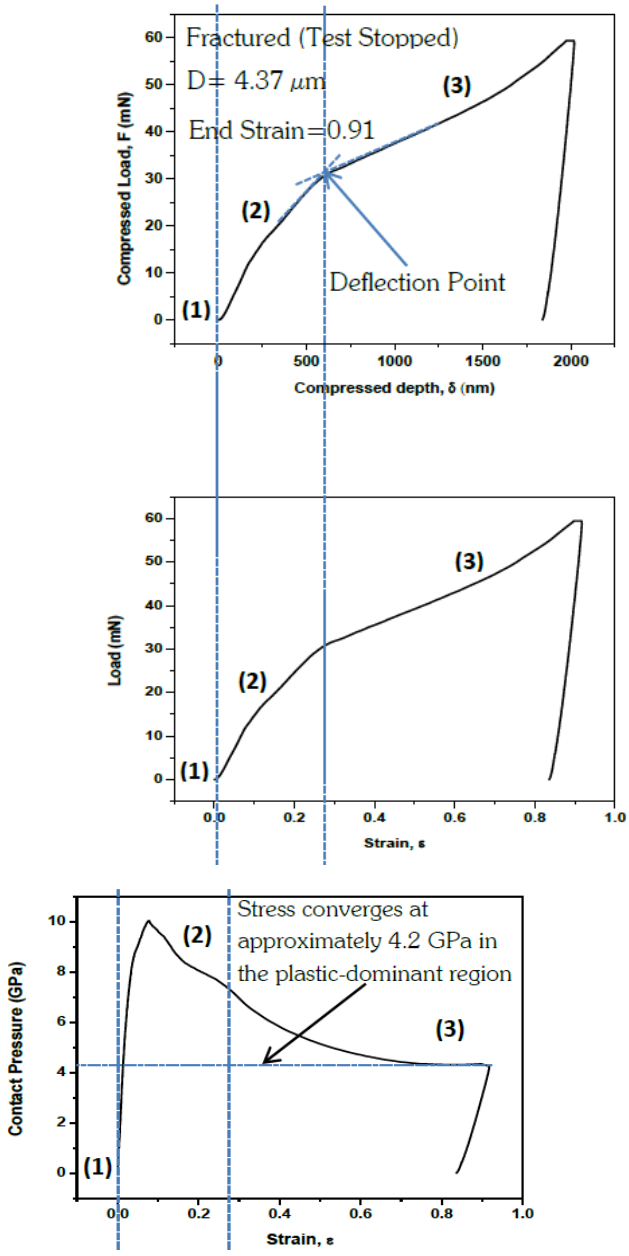

Fig. 12. Stage one shows nose effect of the indenter tip (2) Elastic-plastic deformation stage. Deflection point was observed that separate the Elastic-plastic from the plastic region. (3) Dominantly plastic deformation.

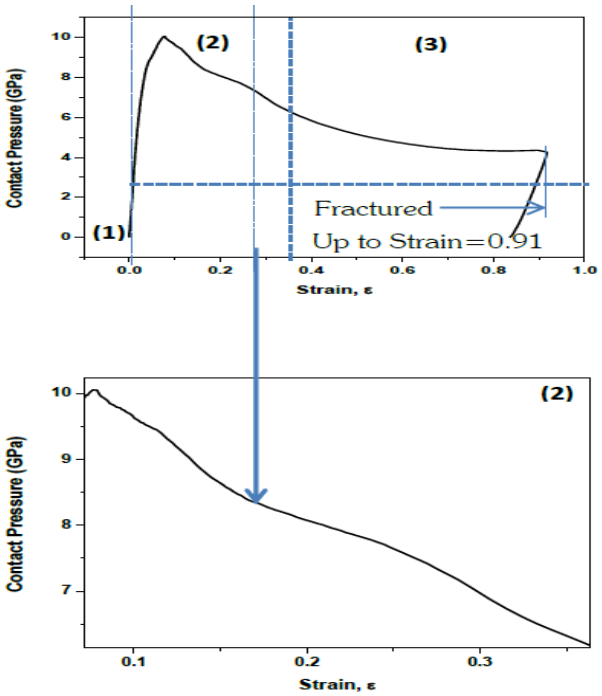

Fig. 13. The elastically deformed zone decreases with increasing strain, and become much smaller than the zone with plastic deformation in (2). The early stage of (2), shows a sharp pressure drop with no pop-in event.

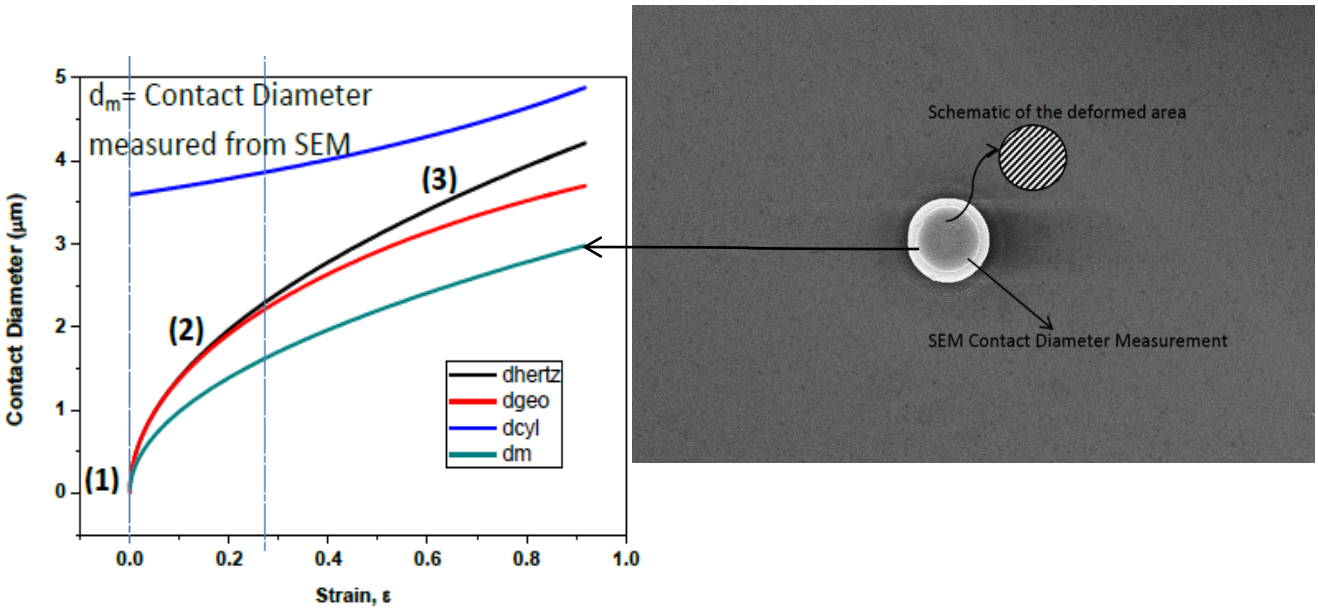

Fig. 14. (2) Elastic-plastic deformation stage, the contact diameter of the particle increased with increase in strain as compared to the other three contact models. However, it was seen in the plastic domain region (3) that the contact diameter of the particle changes almost linearly with the strain (this is where the particle takes the barrel shape).

IV. Conclusion

By using a nanoindentation-based flat punch test method, the mechanical properties and behavior of four groups of amorphous micron-sized particles have been studied. A clear distinction between the elastic-plastic and plastic regime has been probed. A deflection point was observed in the load-strain graph. The particles are made of same chemical compositions but different sizes, 3.36 µm, 4.39 µm, 7.19 µm and 10.05 µm. The contact pressure –strain curves are calculated from the indentation load–displacement results. The contact pressure–strain behavior up to 20 %, 30 % and 40 % deformation is considered. Cracks in meridian planes exhibit slabbing or axial splitting and seem to be guided around a core structure. A shape pressure drop was observed in the contact pressure-strain behavior of the particle. The elastic range is seen to be much smaller as compared to the plastic range. Stress converges at approximately 4.2 GPa in the plastic-dominant region which shows a ductile failure. The results demonstrate that contact pressure–strain behavior of the amorphous particles in the plastic regime have significant size dependence: the smaller the size, the harder the particles behaves.

Acknowledgement

The authors acknowledge Shenyang National Laboratory for Material Science, Institute of Metal Research, Chinese Academy of Sciences, for sponsoring this research.

References

[1] [1] K. L. Johnson, Contact Mechanics, Cambridge University Press, Cambridge, U.K., 1985.

[2] [2] A. C. Fischer-Cripps, Introduction to Contact Mechanics, 2nd ed., 2007, Springer Science Business Media, LLC, ISBN 0-387-68187-6.

[3] [3] J. Y. He, Z.L.Zhang, H.Kristiansen, compression properties of individual micron-sized acrylic particles, Elsevier B.V., material letters 63 (2009) 1696-1698.

[4] [4] J. Y. He, S. Nagao, H. Kristiansen, Z. L. Zhang, loading rate effects on the fracture of Ni/Au nano-coated acrylic particles. Express Polymer Letters, Vol.6, No.3 (2012) 198-203.

[5] [5] J. Y. He, Z. L. Zhang, H. Kristiansen, nanomechanical characterization of single micron-sized polymer particles, journ7al of applied polymer science, Vol.113, 1398-1405 (2009).

[6] [6] Ailian Chen, Weibin Mu, Yang Chen, compressive elastic moduli and polishing performance of non-rigid core/shell structured PS/SiO2 composite abrasives evaluated by AFM, applied surface science 290 (2014) 433-439. Elservier.

[7] [7] J.Paul, S.Romeis, M. Mackovic, V.R.R. Marthala, P.Herre, T.Przybilla, M.Hartmann, E.Spiecker, J. Schmidt, W. Peukert, in situ cracking of silica beads in the SEM and TEM-effect of particle size on structure-property correlations. Powder technology 270 (2015) 337-347.

[8] [8] V.B.Nguyen, C.X.Wang, C.R.Thomas, Z.Zhang, mechanical properties of single alginate microspheres determined by microcompression and finite element modelling, chemical engineering science 64 (2009) 821-829. Elservier.

[9] [9] Y. Xia, M. Bigerelle, S. Bouvier, A. Iost, P.E. Mazeran, quantitative approach to determine the mechanical properties by nanoindentation test: application on sand blasted materials, tribology international 82 (2015) 297-304. Elservier.

[10] [10] S. Naderi, M. A. Hassan7, A. R. Bushroa, alternative methods to determine the elastoplastic properties of sintered hydroxyapatite from nanoindentation testing, materials and design 67 (2015) 360-368. Elservier.

[11] [11] Jonas 1Paul, Stefan Romeis, Jurgen Tormas, Wolfgang Peukert, A review of models for single particle compression and application to silica microspheres, advanced powder technology 25 (2014) 136-153. Elservier.

[12] [12] J. Y. He, Z. L. Zhang, M. Midttun, G. Fonnum, G.I. Modahl, H. Kristiansen, K. Redford, size effect on7 mechanical properties of micron7-sized PS-DVB 1polymer particles, polymer 49 (2008) 3993-3999.

[13] [13] W.M. Mook, J.D. Nowak, C.R. Perrey, C.B. Carter, R. Mukherjee, S.L. Girshick, et al., Compressive stress effects on nanoparticle modulus and fracture, Physical Review B 75 (2007) 214112.

[14] [14] W.M. Mook, C. Niederberger, M. Bechelany, L. Philippe, J. Michler, Compression of freestanding gold nanostructures: from stochastic yield to predictable flow, Nanotechnology 21 (2010) 055701.

[15] [15] Junhua Zhao, Shijo Nagao, Gregory M Odegard, Zhiliang Zhang, Helge Kristiansen, Jianying He, size-dependent mechanical behaviour of nanoscale polymer particles through coarse-grained molecular dynamics simulation, nanoscale research letters 2013, 8:541.

[16] [16] Zhang-Jie Wang, Qing-Jie Li, Zhi-Wei Shan, Ju Li, Jun Sun, Evan Ma, sample size effects on the large strain bursts in submicron aluminium pillars, applied physics letters 100, 071906 (2012).

[17] [17] Nix W.D, Gao H. J Mech Phys Solids 1998; 46:411.

[18] [18] Gerberich WW, Tymiak NI, Grunlan JC. J Appl Mech 2002; 69:433.

[19] [19] Jonas Paul, Stefan Romeis, Jurgen Tomas, Wolfgang Peukert, A review of models for single particle compression and their application to silica microspheres, Advanced Powder Technology 25 (2014) 136–153. Elservier.

[20] [20] H. Hertz, Ueber die Berührung fester elastischer Körper, Journal für die reineund angewandte Mathematik (Crelle's Journal) (1882) 156–171.

[21] [21] H. Hertz, "On the contact of elastic solids," J. Reine Angew. Math. 92, 1881, pp. 156–171. Translated and reprinted in English in Hertz's Miscellaneous Papers, Macmillan & Co., London, 1896, Ch. 5.

[22] [22] H. Hertz, "On hardness," Verh. Ver. Beforderung Gewerbe Fleisses 61, 1882, p. 410. Translated and reprinted in English in Hertz's Miscellaneous Papers, Macmillan &Co, London, 1896, Ch. 6.

[23] [23] Sergiy Antonyuk, Jurgen Tomas, Stefan Heinrich, Lothar Morl, b4reakge b4ehaviour of spherical granulates by compression, chemical engineering science 60 (2005) 4031-4044.

[24] [24] W.C. Oliver and G.M. Pharr, "An improved technique for determining hardness and elastic modulus using load and displacement sensing indentation experiments," J. Mater. Res., 7 4, 1992, pp. 1564–1583.

[25] [25] Pethica, J. B. and Oliver, W. C., (1989), Mat. Res. Soc. Symp. Proc. 130, 13.

[26] [26] K.L. Johnson, K. Kendall, A.D. Roberts, Surface energy and the contact of elastic solids, Proceedings of the Royal Society of London. Series A, Mathematical and Physical Sciences 324 (1971) 301–313.

[27] [27] E.J. Abbott, F.A. Firestone, Specifying surface quality: a method based on accurate measurement and comparison, Mechanical Engineering 55 (1933) 569.

[28] [28] I. Etsion, Y. Kligerman, Y. Kadin, Unloading of an elastic–plastic loaded spherical contact, International Journal of Solids and Structures 42 (2005) 3716–3729.

[29] [29] L.-Y. Li, C.-Y. Wu, C. Thornton, A theoretical model for the contact of elastoplastic bodies, Proceedings of the Institution of Mechanical Engineers, Part C: Journal of Mechanical Engineering Science 216 (2002) 421–431.

[30] [30] K.L. Johnson, An experimental determination of the contact stresses between plastically deformed cylinders and spheres, in: J. Heyman, F.A. Leckie (Eds.), Engineering Plasticity, Cambridge University Press, Cambridge, 1968, pp. 341–461.

[31] [31] Y.H. Lee, J.H. Hahn, S.H. Nahm, J.I. Jang, D. Kwon, Investigations on indentation size effects using a pile-up corrected hardness, Journal of Physics D: Applied Physics 41 (2008) 074027.

[32] [32] J.Y. He , Z.L. Zhang , M. Midttun , G. Fonnum, G.I. Modahl , H. Kristiansen , K. Redford , Size effect on mechanical properties of micron-sized PS–DVB polymer particles, Polymer 49 (2008) 3993–3999.

[33] [33] Dan Mordehai, Seok-Woo Lee, Bjorn Backes , David J. Srolovitz , William D. Nix , Eugen Rabkin, Size effect in compression of single-crystal gold microparticles, Acta Materialia 59 (2011) 5202–5215.

[34] [34] B.E. Schuster, Q. Wei, T.C. Hufnagel, K.T. Ramesh, size-independent strength and deformation mode in compression of a Pd-based metallic glass, Acta Materialia 56 (2008) 5091–5100.

[35] [35] K.B. Carlisle, K.K Chawla, G.M.Gladysz, M. Koopman, structure and mechanical properties of micro and macro balloons: an overview of test techniques, J Mater SCI 41 (2006) 3961-3972.

[36] [36] C. X. Wang, C. Cowen, Z. Zhang, C.R. Thomas, high-speed compression of single alginate microspheres, chemical engineering science 60 (2005) 6649-6657.

[37] [37] Luciane Ribas, Guilherme C. Cordeiro, Romildo D. Toledo Filho, Luis Marcelo Tavares, measuring the strength of irregularly-shaped fine particles in a microcompression tester, minerals engineering 65 (2014) 149-155.

[38] [38] J.P. Chu, C. L. Chiang, H. Wijaya, R.T. Huang, C.W. Wu, B. Zhang, W. H. Wang and T. G. Nieh, compressive deformation of a bulk Ce-based metallic glass, scripta materialia 55 (2006) 227-230.

[39] [39] C.L. Chiang, J.P. Chu, C.T. Lo, T. G. Nieh, Zhi Xin Wang, Wei Hua Wang, homogeneous plastic deformation in a Cu-based bulk amorphous alloy, intermetallics 12 (2004) 1057-1061.

[40] [40] J.P. Chu, C. L. Chiang, T. G. Nieh, Y. Kawamura, superplasticity in a bulk amorphous Pd-40Ni-20P alloy: a compression study, intermetallics 10 (2002) 1191-1095.

[41] [41] Zhang-Jie Wang, Qing-Jie Li, Zhi-Wei Shan, Ju Li, Jun Sun, Evan Ma, sample size effect on large strain bursts in submicron aluminum pillars, applied physics letters 100, 071906 (2012).

[42] [42] Jan Schroers and William L. Johnson, ductile bulk metallic glass, physical review letters 93, 255506 (2004).

[43] [43] H.Bei, S. Xie, E. P. George, softening caused by profuse shear banding in bulk metallic glass, physical review letters 96, 105503 (2006)

AUTHORS

First Author – S.O.B Oppong, Regional Maritime University, Ghana
Second Author – L. Gyansah, Regional Maritime University, Ghana
Third Author – Michael Acquaye, Regional Maritime University, Ghana

Corresponding Authors: samuel.oppong@rmu.edu.gh, gyansahaclass@yahoo.com and michaelappiahacquaye@gmail.com